

Development of Mg-14Ni-6TaF₅ Hydrogen Absorption-Desorption Material via Reaction-Involved Milling

Myoung Youp SONG^{1*}, Young Jun KWAK², Seong Ho LEE², Hye Ryoung PARK³

¹ Division of Advanced Materials Engineering, Research Center of Advanced Materials Development, Engineering Research Institute, Chonbuk National University, 567 Baekje-daero Deokjin-gu, Jeonju, Chonbuk, 561-756, South Korea

² Department of Materials Engineering, Graduate School, Chonbuk National University, 567 Baekje-daero Deokjin-gu, Jeonju, Chonbuk, 561-756, South Korea

³ School of Applied Chemical Engineering, Chonnam National University, 300 Yongbong-dong Buk-gu, Gwangju, 500-757, South Korea

crossref <http://dx.doi.org/10.5755/j01.ms.20.4.6457>

Received 14 February 2014; accepted 02 May 2014

A sample with 80 w/o Mg-14 w/o Ni-6 w/o TaF₅ composition (named Mg-14Ni-6TaF₅) was prepared by reaction-involved milling. The hydrogen absorption and release characteristics of the sample were then investigated. Activation of the sample was finished after two absorption (at 1.2 MPa hydrogen)-desorption (in vacuum) cycles. The activated Mg-14Ni-6TaF₅ had a useful hydrogen absorption-desorption capacity approaching 6 w/o at 573 K at 1.2 MPa hydrogen. At 573 K, the activated sample stored 4.98 w/o hydrogen during 5 min, 5.42 w/o hydrogen during 10 min, and 5.74 w/o hydrogen during 60 min at 1.2 MPa hydrogen, and desorbed 0.15 w/o hydrogen during 5 min, 0.37 w/o hydrogen during 10 min, 1.18 w/o hydrogen during 30 min, and 2.22 w/o hydrogen during 60 min at 0.1 MPa hydrogen. The activated sample absorbed hydrogen at a comparatively low temperature of 423 K (3.59 w/o hydrogen in the fifth cycle during 60 min at 1.2 MPa hydrogen).

Keywords: hydrogen absorption-desorption material; magnesium; Ni and TaF₅ addition; reaction-involved milling; hydrogen absorption and release rates.

1. INTRODUCTION

There are some hydrogen storage methods such as pressure storage, cryogenic storage, carbon nanotube storage, and metal hydride storage. The metal hydride storage possesses some advantages over other hydrogen storage methods from the viewpoints of per unit volume absorption-release capacity, safety, utilization cost, and usability [1, 2].

Magnesium is one of the lightest metals [3–7] and possesses many merits as a hydrogen absorbing material considering the aspect of hydrogen absorption-desorption capacity, price, and reserves in the earth [8]. However, it has very low hydrogen storage and release rates.

Substantial research to increase the hydrogen absorption and release rates of magnesium has been conducted by alloying magnesium with other metals [9–27].

Reilly et al. [9] and Friedlmeier et al. [10] raised hydrogen absorption and release rates of magnesium by adding nickel. Song et al. [28] ground mechanically Mg with Ni in Ar, Bobet et al. [29] prepared cobalt, nickel, or iron-containing mixtures by milling mechanically under hydrogen (reaction-involved milling).

de Castro et al. [30] increased hydrogen absorption and release rates of Mg by milling mechanically nanostructured MgH₂, with incorporating small quantities of FeF₃.

Kim et al. [31] prepared a sample of MgH₂ containing 1 mol% NbF₅ by high-energy ball grinding. They reported

that after 10 absorption-desorption cycles, noncrystalline Nb-F phase was changed into crystalline Nb hydrides, which probably played a decisive role in increasing the absorption and release rates of MgH₂.

Malka et al. [32] studied the effects of different halide additives milled with magnesium hydride (MgH₂) on its desorption temperature. They reported that, from the halides investigated, the best catalysts for magnesium hydride desorption were ZrF₄, TaF₅, NbF₅, VCl₃, and TiCl₃. Malka et al. [33] milled MgH₂ with 7 w/o of various metal halide additives (ZrF₄, TaF₅, NbF₅, and TiCl₃). They reported that the catalytic effect of metal halides on the Mg hydrogen absorption/desorption process resulted from making pure transition metal and/or the MgF₂ phase.

Magnesium fabricated by mechanical milling in hydrogen (reaction-involved milling) with transition elements or oxides exhibited comparatively high absorption and desorption rates when the content of addition agents was 20 w/o around.

In the present study, Ni and TaF₅ were chosen as addition agents to raise the absorption and release rates of Mg. A sample with an 80 w/o Mg-14 w/o Ni-6 w/o TaF₅ composition, which contained 20 w/o addition agents, was prepared by reaction-involved milling. The hydrogen storage and release characteristics of the sample were then investigated. The sample was named Mg-14Ni-6TaF₅.

2. EXPERIMENTAL DETAILS

The materials used for sample preparation were pure Mg powder (particle size 74 μm–149 μm, purity 99.6 %, Alfa Aesar), Ni (Nickel powder APS, 2.2 μm–3.0 μm,

* Corresponding author. Tel.: +82-63-270-2379, fax: +82-63-270-2386. E-mail address: songmy@jbnu.ac.kr (M. Y. Song)

purity 99.9 % metal basis, C typically < 0.1 %, Alfa Aesar), and TaF₅ (Tantalum (V) fluoride, purity 98 %, Aldrich).

Reaction-involved milling was conducted in a planetary ball mill (Planetary Mono Mill; Pulverisette 6, Fritsch). The total weight of a mixture having the desired composition was 8 g. 105 hardened steel balls (total weight = 360 g, 45 times of the sample weight) were used. All sample treatment was done in an Ar-filled glove box. The mill container with a volume of 250 ml was filled with high purity hydrogen gas of about 1.2 MPa. The disc revolution speed was 250 rpm. The reaction-involved milling time was 6 h; the time was composed of alternating cycles of 20 min that had milling for 15 min and a rest period of 5 min. Hydrogen was refilled every two hours.

The variation of the stored or released hydrogen amount with time was measured under nearly constant hydrogen pressure, employing a Sievert's type hydrogen absorption and desorption apparatus, which was previously described [34]. The quantity of the sample used for these measurements was 0.5 g.

X-ray diffraction (XRD) diagrams of the samples after reaction-involved milling and after absorption-desorption cycling were acquired with a Rigaku D/MAX 2500 powder diffractometer utilizing Cu K α radiation. The diffraction angle range was between 10° and 80° and the scan speed was 4° min⁻¹. XRD diagrams were analyzed using program MDI JADE 5.0. The scanning electron microscope (SEM) micrographs of the samples were obtained using JSM-6400 SEM operated at 20 kV. The elements contained in the sample particles after reaction-involved milling and after absorption-desorption cycling were analyzed through line scanning with an energy dispersive X-ray spectrometer (EDS, EDAX).

3. RESULTS AND DISCUSSION

The hydriding reaction of magnesium can be classified by the following steps: transfer of hydrogen molecules to the surface of particles, chemisorption of H₂ molecules on the surface of particles, transition of hydrogen atoms from the chemisorbed state to the absorbed state, and nucleation of magnesium hydride and growth. If a continuous layer of magnesium hydride is formed, diffusion of hydrogen atoms through a growing hydride layer occurs, and then phase transformation from α Mg-H solid solution to magnesium hydride at the magnesium hydride- α Mg-H solid solution interface takes place.

The dehydriding reaction of magnesium hydride can be classified in the reverse sequence of the hydriding reaction of magnesium: nucleation of α Mg-H solid solution, transition of hydrogen atoms from the absorbed state to the chemisorbed state, and transfer of hydrogen molecules from the surface of α Mg-H solid solution. If nuclei grow and a continuous layer of α Mg-H solid solution layer is formed, take place phase transformation from magnesium hydride to α Mg-H solid solution at the magnesium hydride- α Mg-H solid solution interface, diffusion of hydrogen atoms through a growing α Mg-H solid solution layer, transition of hydrogen atoms from the absorbed state to the chemisorbed state, and transfer of hydrogen molecules from the surface of α Mg-H solid solution.

The hydriding and dehydriding reactions of Mg₂Ni can also be classified in the similar way.

Stored hydrogen percentage, H_a , is defined by adopting the weight of sample as a criterion. The H_a versus time t curves showed that the absorption rate of Mg-14Ni-6TaF₅ was high until about 10 min, and very low after 30 min. Until about 10 min, Mg₂Ni, with a higher absorption rate than magnesium, and magnesium particles with small sizes are deemed to have been hydrided and hydrogen is deemed to have been absorbed in the outer part of comparatively large magnesium particles. After about 30 min, it is posited that the hydrogen absorption reaction took place in the interior of comparatively large magnesium particles.

Fig. 1 shows the change in H_a for 30 min (referred to as H_a (30 min)) of Mg-14Ni-6TaF₅ according to cycle number, n , at 553 K, 573 K and 593 K at 1.2 MPa hydrogen. After absorption reaction measurements, hydrogen was released from the samples at each temperature at 0.1 MPa hydrogen and subsequently in a vacuum. At 553 K H_a (30 min) reaches its maximum value at $n = 3$, and at 573 K, the maximum value is reached at $n = 2$. At 593 K, H_a (30 min) reaches its maximum value at $n = 4$, which is very similar to those at $n = 3$ and $n = 2$. These results show that activations of the samples were completed after two cycles of absorption (at 1.2 MPa hydrogen)-desorption (in vacuum). The activation is a process, which enables the sample to have the highest hydriding and dehydriding rates and is performed by repeating the absorption-desorption cycle. The particles of the activated sample have very reactive clean surfaces, are very small, and have many defects.

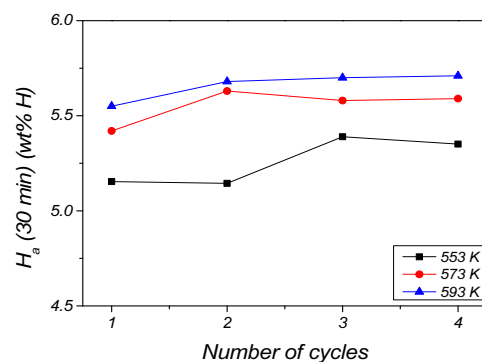


Fig. 1. Change in H_a during 30 min, H_a (30 min), of Mg-14Ni-6TaF₅ according to cycle number, n , at 553 K, 573 K and 593 K at 1.2 MPa hydrogen

The change in H_a versus t curve according to temperature (423 K, 523 K, 553 K, 573 K, 593 K, and 623 K) at 1.2 MPa hydrogen for the activated Mg-14Ni-6TaF₅ is shown in Fig. 2. At a relatively low temperature of 423 K, the activated sample has a fairly high absorption rate, absorbing 3.05 w/o hydrogen during 5 min, 3.22 w/o hydrogen during 10 min, 3.46 w/o hydrogen during 30 min, and 3.59 w/o hydrogen during 60 min at 1.2 MPa hydrogen. At the beginning of the absorption reaction, the absorption rate is extremely high, and then gets lower after about 10 min. The initial absorption rate increases as the temperature is raised from 423 K to 573 K, and then decreases with a further increase of temperature from 573 K to 623 K. The increase in temperature has two effects; acceleration of

thermally activated process (such as diffusion of hydrogen atoms through growing hydride layer) and decrease in the driving force for the hydriding reaction, which is related to the difference between the applied hydrogen pressure (1.2 MPa hydrogen) and the equilibrium plateau pressure at a reaction temperature. When the temperature increases from 423 K to 573 K, the effect of the acceleration of the thermally activated process is believed to predominate, leading to the increase in the hydriding rate. When the temperature increases from 573 K to 623 K, the effect of the decrease in the driving force for hydriding reaction is believed to predominate, leading to the decrease in the hydriding rate with temperature. The H_a value during 60 min increases as the temperature increases from 423 K to 593 K, and decreases from 593 K to 623 K. The Mg_2Ni phase is produced in the $Mg-14Ni-6TaF_5$ sample after absorption-desorption cycling. In the early stage of the H_a versus t curves, Mg_2Ni , with a higher absorption rate than magnesium, and magnesium particles with small sizes are deemed to be hydrided and hydrogen is deemed to be absorbed in the outer part of comparatively large magnesium particles. In the later stage of H_a versus t curves, it is posited that the hydrogen absorption reaction takes place in the interior of comparatively large magnesium particles.

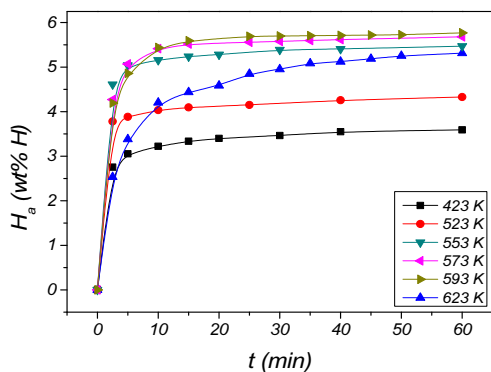


Fig. 2. Change in H_a versus t curve according to temperature (423 K, 523 K, 553 K, 573 K, 593 K and 623 K) at 1.2 MPa hydrogen of activated $Mg-14Ni-6TaF_5$

The released hydrogen percentage, H_d , is also expressed by adopting the sample weight as a criterion. Fig. 3 exhibits the H_a versus t curves at 1.2 MPa hydrogen and the H_d versus t curves at 0.1 MPa hydrogen at 573 K and 593 K for the activated $Mg-14Ni-6TaF_5$ (at $n = 2$). The H_a versus t curves show that the initial absorption rates are very high (1.71 wt% hydrogen/min at 573 K) and this sample has a fairly large hydrogen absorption-desorption capacity, absorbing 5.74 w/o hydrogen at 573 K during 60 min. The H_d versus t curve at 573 K shows that the H_d varies almost linearly with time. The initial release rate at 593 K is quite high (0.31 wt% hydrogen/min), decreases gradually, and is very low after 30 min. The much higher absorption rate than the release rate at 573 K is due to the much higher driving force for absorption (1.039 MPa hydrogen) than that for release (0.061 MPa hydrogen). The sample absorbs 4.98 w/o hydrogen during 5 min, 5.42 w/o hydrogen during 10 min, 5.60 w/o hydrogen during 25 min, and 5.74 w/o hydrogen during 60 min at 573 K at 1.2 MPa hydrogen, and desorbs 0.15 w/o hydrogen during 5 min, 0.37 w/o hydrogen during 10 min, 1.18 w/o hydrogen

during 30 min, and 2.22 w/o hydrogen during 60 min at 573 K at 0.1 MPa hydrogen. We define a useful hydrogen absorption-desorption capacity as the quantity of hydrogen stored during 60 min. The activated $Mg-14Ni-6TaF_5$ has a useful hydrogen absorption-desorption capacity near 6 w/o at 573 K at 1.2 MPa hydrogen.

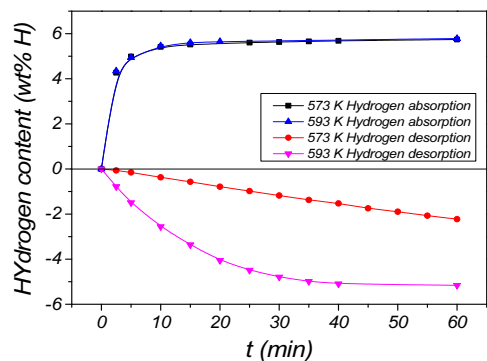


Fig. 3. H_a versus t curves at 1.2 MPa hydrogen and H_d versus t curves at 0.1 MPa hydrogen at 573 K and 593 K of activated $Mg-14Ni-6TaF_5$ (at $n = 2$)

The XRD diagram of $Mg-14Ni-6TaF_5$ after reaction-involved milling is shown in Fig. 4. The sample contains Ni (JCPDS card number 45-1027), Mg (35-0821), $\beta-MgH_2$ (12-0697), and $\gamma-MgH_2$ (35-1184). $\beta-MgH_2$ and $\gamma-MgH_2$ are formed during reaction-involved milling by the reaction of Mg with hydrogen. $\beta-MgH_2$ is a room temperature form of MgH_2 , and $\gamma-MgH_2$ is a high pressure form of MgH_2 . The XRD diagram of $Mg-14Ni-6TaF_5$ after reaction-involved milling exhibits a little stronger background and broader peaks than those of the XRD diagram of $Mg-14Ni-6TaF_5$ after absorption-desorption cycling at 593 K ($n = 4$). The XRD diagram of $Mg-14Ni-6TaF_5$ after absorption-desorption cycling ($n = 4$) revealed the phases of Mg, Mg_2Ni , $\beta-MgH_2$, and small amounts of MgO , MgF_2 , and Ta_2H .

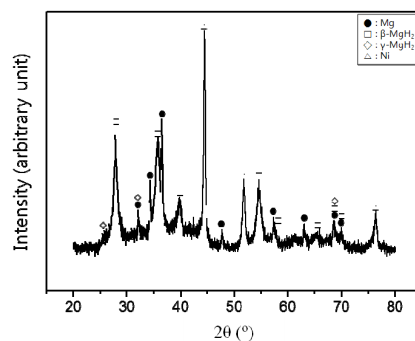


Fig. 4. XRD diagram of $Mg-14Ni-6TaF_5$ after reaction-involved milling

The SEM micrographs of $Mg-14Ni-6TaF_5$ after reaction-involved milling and after absorption-desorption cycling at 593 K ($n = 4$) were obtained. The particle sizes of the $Mg-14Ni-6TaF_5$ after reaction-involved milling were not homogeneous. The particle sizes of the $Mg-14Ni-6TaF_5$ after absorption-desorption cycling at 593 K ($n = 4$) were not homogeneous, either. The particles were smaller than those of $Mg-14Ni-6TaF_5$ after reaction-involved milling. The expansion of the particles due to hydrogen

absorption and the contraction of the particles due to hydrogen release is believed to lead to the decrease in the particle size.

The sample after absorption-desorption cycling at 593 K ($n=4$) had smaller particle size than that after reaction-involved milling. The XRD diagram of Mg-14Ni-6TaF₅ after reaction-involved milling exhibits a little stronger background and broader peaks than those of the XRD diagram of Mg-14Ni-6TaF₅ after absorption-desorption cycling at 593 K ($n=4$). The strong background and broad peak result from fine particle size and/or amorphousness of particles. These two results indicate that the MgH₂-6Ni-6TaF₅ after reaction-involved milling is slightly amorphous.

The back-scattered electrons (BSE) image and line scanning result by EDS for Mg-14Ni-6TaF₅ after reaction-involved milling were obtained. The composition along a scanned line for the sample after reaction-involved milling was O: 37.35 w/o, F: 1.89 w/o, Ni: 3.31 w/o, Mg: 55.08 w/o, and Ta: 2.36 w/o.

The BSE image and line scanning result by EDS for Mg-14Ni-6TaF₅ after absorption-desorption cycling ($n=4$) are shown in Fig. 5. The particles after absorption-desorption cycling are smaller than those of Mg-14Ni-6TaF₅ after reaction-involved milling. The composition along the scanned line for the sample after absorption-desorption cycling is O: 5.46 w/o, F: 1.51 w/o, Ni: 3.39 w/o, Mg: 88.14 w/o, and Ta: 1.51 w/o. The appearances of Ta and F peaks at different positions in Fig. 5 show that TaF₅ is decomposed after reaction-involved milling and after absorption-desorption cycling.

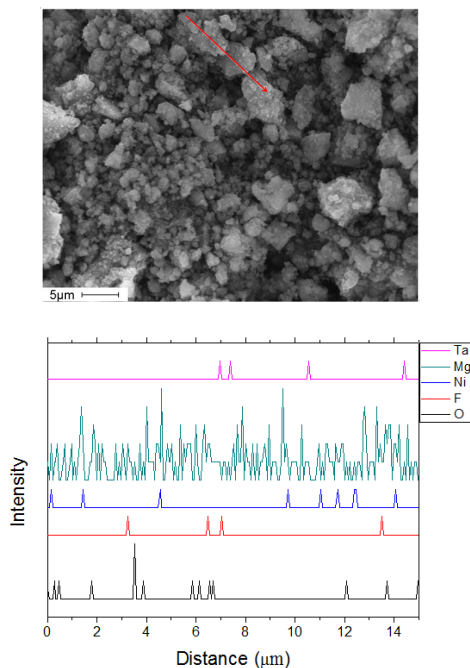
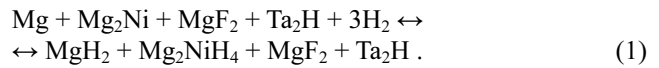


Fig. 5. Back-scattered electrons (BSE) image and line scanning result by EDS for Mg-14Ni-6TaF₅ after absorption-desorption cycling ($n=4$)

The sample dehydrided at the 4th hydriding-dehydriding cycle contained Mg, Mg₂Ni, β -MgH₂, and small amounts of MgO, MgF₂, and Ta₂H. Mg₂Ni was formed by the reaction of Mg and Ni during hydriding-

dehydriding cycling. γ -MgH₂ was decomposed, and MgO was formed by the reaction of Mg with the oxygen that was probably contained in the hydrogen as an impurity, during hydriding-dehydriding cycling. From the results of Fig. 4 and Fig. 5, the following reactions are believed to occur among Mg, Mg₂Ni, MgF₂, Ta₂H, and hydrogen during subsequent hydriding and dehydriding reactions:



The Mg₂Ni phase produced in the Mg-14Ni-6TaF₅ sample after absorption-desorption cycling. Dimagnesium nickel has higher absorption and desorption rates than magnesium. The incorporation of Ni raises not only the absorption rate of magnesium, but also the desorption rate of MgH₂ by forming Mg₂Ni from the reaction of Ni with Mg during absorption-desorption cycling. The reaction-involved milling of Mg with TaF₅ raises the storage and release rates, and the incorporation of TaF₅ is thought to make defects outside and inside magnesium particles, leading to the facilitation of nucleation, and to decrease the magnesium particle size, leading to the diminution of the diffusion distances for hydrogen atoms.

During hydriding, magnesium and dimagnesium nickel, Mg₂Ni, expand, and during dehydriding, they contract. The increase in the absorption and release rates during activation and the variation of the microstructure with cycling, indicate that the absorption-desorption cycling also raises the absorption and release rates of magnesium by promoting nucleation (by making defects outside the Mg particles) and by shortening the diffusion distances of hydrogen atoms (by producing cracks outside the magnesium particles and decreasing the particle size of magnesium).

4. CONCLUSIONS

A sample with 80 w/o Mg-14 w/o Ni-6 w/o TaF₅ composition was prepared by reaction-involved milling, and its hydrogen storage and release characteristics were then investigated. The activated Mg-14Ni-6TaF₅ had a fairly high absorption rate and a large hydrogen absorption-desorption capacity with an effective hydrogen absorption-desorption capacity of near 6 w/o. The activated Mg-14Ni-6TaF₅ absorbed 5.74 w/o hydrogen at 1.2 MPa hydrogen and desorbed 2.22 w/o hydrogen at 0.1 MPa hydrogen at 573 K during 60 min. Activation of the sample was finished after two absorption (at 1.2 MPa hydrogen)-desorption (in vacuum) cycles. At 573 K, the activated sample absorbed 4.98 w/o hydrogen during 5 min, 5.42 w/o hydrogen during 10 min, 5.60 w/o hydrogen during 25 min, and 5.74 w/o hydrogen during 60 min at 1.2 MPa hydrogen, and desorbed 0.15 w/o hydrogen during 5 min, 0.37 w/o hydrogen during 10 min, 1.18 w/o hydrogen during 30 min, and 2.22 w/o hydrogen during 60 min at 0.1 MPa hydrogen. The incorporation of nickel raises not only the absorption rate of magnesium but also the release rate of magnesium hydride, by producing dimagnesium nickel during absorption-desorption cycling. The reaction-involved milling of Mg with TaF₅ increases the storage and release rates, and the incorporation of TaF₅ is thought to make defects outside and inside the magnesium particles,

leading to the facilitation of nucleation, and to decrease the particle size of magnesium, leading to the diminution of the diffusion distances for hydrogen atoms. During the absorption reaction, magnesium and dimagnesium nickel expand, and during the desorption reaction, they contract. The increase in storage and release rates during the activation and the variation of the microstructure with cycling indicate that the absorption-desorption cycling also raises the absorption and desorption rates of Mg by promoting nucleation and making shorter the diffusion distances of hydrogen atoms.

Acknowledgments

This research was supported by Basic Science Research Program through the National Research Foundation (NRF) of Korea funded by the Ministry of Education, Science and Technology (Grant number 2011-0023566). This work was also supported by the selection of research-oriented professor (Song M. Y.) of Chonbuk National University in 2013.

REFERENCES

1. Song, M. Y., Kwak, Y. J., Lee, S. H., Park, H. R., Kim, B. G. Improvement of Hydrogen-storage Properties of MgH₂ by Addition of Ni and Ti via Reactive Mechanical Grinding and a Rate-controlling Step in Its Dehydrogenation Reaction *Metals and Materials International* 19 (4) 2013: pp. 879–885.
2. Hong, S. H., Song, M. Y. Fabrication of Fe-Ti Alloys by Pulsed Current-assisted Reaction from Iron, Manganese and Titanium Oxide or Titanium Hydride *Metals and Materials International* 19 (4) 2013: pp. 895–899.
3. Moon, B. G., You, B. S., Koh, K. H. Recycling Technology of End-of-life Magnesium Scrap *Korean Journal of Metals and Materials* 51 (1) 2013: pp. 1–14.
4. Yu, J. I., Yoon, J. S., Yoon, J. G., Kim, J. H., Choi, S. D., Jang, H. K., Yu, J. Y., Bae, I. H. Characteristics of the Anodic Films on an AZ91D Mg Alloy Prepared by Plasma Electrolytic Oxidation and Burning Surface Treatment *Korean Journal of Metals and Materials* 51 (6) 2013: pp. 405–412.
5. Nam, S. W., Kim, W. T., Kim, D. H., Kim, T. S. Microstructure and Corrosion Behavior of Rapidly Solidified Mg-Zn-Y Alloys *Metals and Materials International* 19 (2) 2013: pp. 205–209.
6. Guan, R. G., Zhao, Z. Y., Lian, C., Cui, T., Lee, C. S. Microstructure Formation Mechanism and Properties of a Mg-3Sn-1Mn (wt%) Magnesium Alloy Processed by a Novel Semisolid Continuous Shearing and Rolling Process *Metals and Materials International* 19 (1) 2013: pp. 33–38.
7. Lee, B. D., Kim, E. J., Baek, U. H., Han, J. W. Precipitate Prediction Model of Mg-xAl (x = 3, 6, 9) Alloys *Metals and Materials International* 19 (2) 2013: pp. 135–145. <http://dx.doi.org/10.1007/s12540-013-2001-6>
8. Van Phuong, N., Lee, K., Chang, D., Kim, M., Lee, S., Moon, S. Zinc Phosphate Conversion Coatings on Magnesium Alloys: A Review *Metals and Materials International* 19 (2) 2013: pp. 273–281.
9. Reilly, J. J., Wiswall, R. H. Jr. The Reaction of Hydrogen with Alloys of Magnesium and Nickel and the Formation of Mg₂NiH₄ *Inorganic Chemistry* 7 (11) 1968: pp. 2254–2256. <http://dx.doi.org/10.1021/ic50069a016>
10. Friedlmeier, G., Arakawa, M., Hirai, T., Akiba, E. Preparation and Structural, Thermal and Hydrogen Characteristics of Melt-spun Mg-Ni Alloys *Journal of Alloys and Compounds* 292 (1–2) 1999: pp. 107–117.
11. Song, M. Y., Kwon, S. N., Hong, S. H., Park, H. R. Hydrogen Storage Properties of a Ni, Fe and Ti-added Mg-based Alloy *Metals and Materials International* 18 (2) 2012: pp. 279–286.
12. Kwak, Y. J., Park, H. R., Song, M. Y. Hydrogen Absorption by Mg-Ni-Fe₂O₃ and Mg-Ni-Ti during Mechanical Grinding under Hydrogen *Korean Journal of Metals and Materials* 50 (11) 2012: pp. 855–859.
13. Song, M. Y., Baek, S. H., Park, H. R., Mumm, D. R. Effects of Nickel and Iron Oxide Addition by Milling under Hydrogen on the Hydrogen-Storage Characteristics of Mg-Based Alloys *Korean Journal of Metals and Materials* 50 (1) 2012: pp. 64–70.
14. Kwak, Y. J., Lee, S. H., Park, H. R., Song, M. Y. Hydrogen-storage Property Enhancement of Magnesium Hydride by Nickel Addition via Reactive Mechanical Grinding *Korean Journal of Metals and Materials* 51 (8) 2013: pp. 607–613.
15. Song, M. Y., Baek, S. H., Bobet, J.-L., Park, H. R., Kim, B. G. Phase Transformations and Hydrogen-storage Characteristics of Mg-transition Metal-oxide Alloys *Metals and Materials International* 19 (2) 2013: pp. 237–244.
16. Song, M. Y., Kwak, Y. J., Lee, S. H., Park, H. R. Enhancement of Reaction Kinetics with Hydrogen of Mg by Addition of Ni and TaF₅ via Reactive Mechanical Grinding *Korean Journal of Metals and Materials* 51 (1) 2013: pp. 51–55.
17. Lee, S. S., Lee, N. R., Kim, K. I., Hong, T. W. Pressure-composition-isotherm Behaviors of MgH₂-BCY Composites by Reactive Mechanical Alloying *Metals and Materials International* 19 (6) 2013: pp. 1351–1353.
18. Song, M. Y., Kwak, Y. J., Lee, S. H., Park, H. R. Formation of a High Pressure Form of Magnesium Hydride γ-MgH₂ by Mechanical Grinding under Low Hydrogen Pressure *Korean Journal of Metals and Materials* 51 (2) 2013: pp. 119–123.
19. Song, M. Y., Kwon, S. N., Park, H. R., Mumm, D. R. Characterization of a Magnesium-based Alloy after Hydrogen-dehydrogenation Cycling (n = 1–150) *Metals and Materials International* 19 (5) 2013: pp. 1139–1144. <http://dx.doi.org/10.1007/s12540-013-5033-z>
20. Song, M. Y., Kwak, Y. J., Lee, S. H., Park, H. R. Characterization of an MgH₂-Ni Alloy Prepared by Mechanical Grinding under Hydrogen *Korean Journal of Metals and Materials* 51 (4) 2013: pp. 285–290.
21. Hong, S. H., Song, M. Y. Preparation of Mg-33Al Alloy by Rapid Solidification Process and Evaluation of Its Hydrogen-storage Properties *Metals and Materials International* 19 (5) 2013: pp. 1145–1149.
22. Song, M. Y., Kwon, S. N., Kwak, Y. J., Park, H. R., Kim, B. G. Hydrogen-storage Properties of Li₃N, LiBH₄, Fe and/or Ti-added Mg or MgH₂ *Korean Journal of Metals and Materials* 51 (8) 2013: pp. 615–620.
23. Song, M. Y., Kwon, S. N., Mumm, D. R. Hydrogenation Reaction of Mg-Based Alloys Fabricated by Rapid

- Solidification *Metals and Materials International* 19 (2) 2013: pp. 309–314.
24. **Song, M. Y., Kwak, Y. J., Lee, S. H., Park, H. R.** Hydrogen Storage Properties of a Ni and NbF₅-added Mg Alloy *Korean Journal of Metals and Materials* 51 (9) 2013: pp. 671–676.
 25. **Kwak, Y. J., Park, H. R., Song, M. Y.** Comparison of Hydrogen-storage Properties of Mg-14Ni-3Fe₂O₃-3Ti and Mg-14Ni-2Fe₂O₃-2Ti-2Fe *Metals and Materials International* 19 (3) 2013: pp. 543–548.
 26. **Song, M. Y., Kwon, S. N., Park, H. R.** Pressure-composition Isotherms and Cycling Properties of Mg-xFe₂O₃-yNi Alloys *Korean Journal of Metals and Materials* 51 (6) 2013: pp. 455–460.
 27. **Song, M. Y., Kwak, Y. J., Lee, S. H., Park, H. R.** Variations of the Hydriding and Dehydriding Rates of As-milled MgH₂-Ni Alloys with Ni Content *Korean Journal of Metals and Materials* 51 (10) 2013: pp. 761–766.
 28. **Song, M. Y., Darriet, B., Pezat, M., Hagenmuller, P.** Dehydriding Kinetics of a Mechanically Alloyed Mixture with a Composition Mg₂Ni *International Journal of Hydrogen Energy* 12 (1) 1987: pp. 27–30.
[http://dx.doi.org/10.1016/0360-3199\(87\)90123-6](http://dx.doi.org/10.1016/0360-3199(87)90123-6)
 29. **Bobet, J.-L., Chevalier, B., Song, M. Y., Darriet, B., Etourneau, J.** Reactive Mechanical Grinding of Magnesium in Hydrogen and the Effects of Additives *Materials and Manufacturing Processes* 17 (3) 2002: pp. 351–361.
 30. **de Castro, J. F. R., Yavari, A. R., LeMoulec, A., Ishikawa, T. T., Botta, F. W. J.** Improving H-sorption in MgH₂ Powders by Addition of Nanoparticles of Transition Metal Fluoride Catalysts and Mechanical Alloying *Journal of Alloys and Compounds* 389 (1–2) 2005: pp. 270–274.
 31. **Kim, J. W., Ahn, J. P., Jin, S. A., Lee, S. H., Chung, H. S., Shim, J. H., Cho, Y. W., Oh, K. H.** Microstructural Evolution of NbF₅-doped MgH₂ Exhibiting Fast Hydrogen Sorption Kinetics *Journal of Power Sources* 178 2008: pp. 373–378.
<http://dx.doi.org/10.1016/j.jpowsour.2007.12.005>
 32. **Malka, I. E., Czujko, T., Bystrzycki, J.** Catalytic Effect of Halide Additives Ball Milled with Magnesium Hydride *International Journal of Hydrogen Energy* 35 2010: pp. 1706–1712.
 33. **Malka, I. E., Pisarek, M., Czujko, T., Bystrzycki, J.** A Study of the ZrF₄, NbF₅, TaF₅, and TiCl₃ Influences on the MgH₂ Sorption Properties *International Journal of Hydrogen Energy* 36 (20) 2011: pp. 12909–12917.
<http://dx.doi.org/10.1016/j.ijhydene.2011.07.020>
 34. **Bobet, J.-L., Chevalier, B., Song, M. Y., Darriet, B. B.** Improvements of Hydrogen Storage Properties of Mg-based Mixtures Elaborated by Reactive Mechanical Milling *Journal of Alloys and Compounds* 356–357 2003: pp. 570–574.